

Particle motion in a liquid film rimming the inside of a partially filled rotating cylinder

D.D. Joseph, J. Wang, R. Bai, B.H. Yang
Department of Aerospace Engineering and Mechanics
University of Minnesota, Minneapolis, MN 55455

H.H. Hu
Department of Mechanical Engineering and Applied Mechanics
University of Pennsylvania, Philadelphia, PA 19104-6315

March 2003

Abstract

Both lighter- and hydrophobic heavier-than-liquid particles will float on liquid-air surfaces. Capillary forces cause the particles to cluster in typical situations identified here. This kind of clustering causes particles to segregate into islands and bands of high concentrations in thin liquid films rimming the inside of a slowly rotating cylinder partially filled with liquid. A second regime of particle segregation, driven by secondary motions induced by off-center gas bubbles in a more rapidly rotating cylinder at higher filling levels, is identified. A third regime of segregation of bi-disperse suspensions is found in which two layers of heavier-than-liquid particles that stratify when there is no rotation, segregate into alternate bands of particles when there is rotation*.

I. Capillary forces

The deformation of the air-liquid interface due to floating light particles or due to trapped heavy small particles gives rise to capillary forces on the particles. These forces may be qualitatively understood from simple arguments. Three kinds of forces act on particles: forces due to gravity, forces due to the action of contact angles and the pressure forces. These three kinds of forces are at play in the vertical force balance but require a somewhat more elaborate explanation for horizontal force balance. The effects of gravity are usually paramount for heavier-than-liquid floating particles in which one particle will fall into the depression of the second. A heavier-than-liquid particle will fall down a downward sloping meniscus while an

* Movies of the experiments reported in this paper can be viewed at the web address
<http://www.aem.umn.edu/research/particles/rtcylinderpaper/>.

upward buoyant particle will rise. Capillary forces cause particles to cluster, as shown in figure 4.

In this section, we shall review the nature of capillary forces which cause the particles to cluster; in section II we show how these forces produce islands and bands of segregated particles in a thin liquid film rimming the inside of a slowly rotating cylinder.

I-1. Vertical forces

The simplest analysis relevant to understanding the forces on small particles is the vertical force balance on a sphere floating on the interface between fluids which, for convenience, is here called water and air. This analysis was given first by Princen (1969), then by Rapacchietta and Neumann (1977) and by Kotah, Fujita and Imazu (1992), who used the floating ball to measure contact angles.

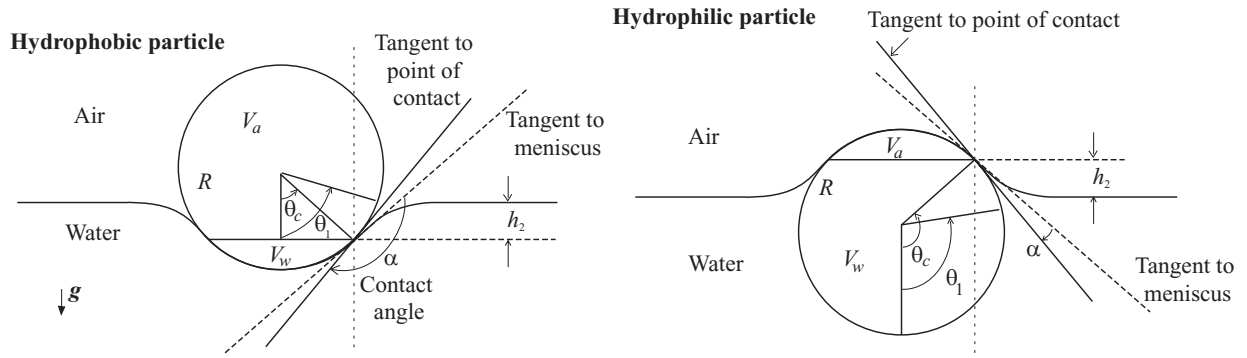


Figure 1. Hydrophobic and hydrophilic particles at equilibrium.

The capillary force F_c is a function of the radius of the particle R , the surface tension coefficient γ , the filling angle (position of the contact ring) θ_c and the contact angle α (see figure 1), given by,

$$F_c = 2\pi(R \sin \theta_c)\gamma \sin[\theta_c - (\pi - \alpha)] = -2\pi R \gamma \sin \theta_c \sin(\theta_c + \alpha) \quad (1)$$

for both the hydrophobic and hydrophilic cases.

At equilibrium, the gravity force G is balanced by the capillary force plus the vertical resultant of pressure around the sphere:

$$F_c + F_p = G \quad (2)$$

where $G = \frac{4}{3}\rho_p \pi R^3 g$. The vertical resultant of pressure around the sphere can be written as

$$F_p = \rho_l g V_w + \rho_a g (V - V_w) - (\rho_l - \rho_a) g h_2 A. \quad (3)$$

where ρ_l and ρ_a are densities of the liquid and the air, respectively; h_2 is the depression generated by the particle, with a negative value in the case shown in figure 1(a) and a positive value shown in figure 1(b); $V = \frac{4}{3} \pi R^3$ is the volume of the sphere, $V_w = \pi R^3 \left(\frac{2}{3} - \cos \theta_c + \frac{1}{3} \cos^3 \theta_c \right)$ is the volume of the sphere immersed in the water and $A = \pi (R \sin \theta_c)^2$ is the area of the contact ring. The first two terms at the right hand side of (3) are in agreement with Archimedes' principle, while the last term accounts for the meniscus effect. When a meniscus is present, the buoyancy calculated by Archimedes' principle $\rho_l g V_w + \rho_a g (V - V_w)$ lifts not only the sphere, but also the liquid cylinder $h_2 A$ above the contact ring.

Inserting (1) and (3) into (2), we get the vertical force balance,

$$\sin \theta_c \sin(\theta_c + \alpha) = -\frac{B}{2} \left[\frac{4}{3} \psi_1 - \left(\frac{2}{3} - \cos \theta_c + \frac{1}{3} \cos^3 \theta_c \right) - \psi_2 \left(\frac{2}{3} + \cos \theta_c - \frac{1}{3} \cos^3 \theta_c \right) \right] + (1 - \psi_2) (\cos \theta_c - \cos \theta_1) \sin^2 \theta_c \quad (4)$$

where $\cos \theta_c - \cos \theta_1 = h_2/R$ and θ_1 is measured from the point of extension of the flat interface as indicated in figure 1. $B = \rho_l R^2 g / \gamma$ is the bond number and $\psi_1 = \rho_p / \rho_l$ and $\psi_2 = \rho_a / \rho_l$ are the dimensionless control parameters.

It can be inferred from (4) that the left side of the equation, consequently, the right side, lies in the range $-1 \leq \sin \theta_c \sin(\theta_c + \alpha) \leq 1$. Obviously this equation cannot be solved if the particles are too large or too heavy. However, it can be concluded that small hydrophobic particles can always be suspended in fluid surfaces no matter how heavy they may be, as long as $\rho_p R^2 g / \gamma$ is small enough. Moreover, in the limit of $\rho_p R^2 g / \gamma \rightarrow 0$, $\sin \theta_c \sin(\alpha + \theta_c) = 0$ and the particles sit on the top of the fluid or are held in place by capillarity.

If the particle is irregular with sharp corners the contact angle argument fails. Liquid-air surfaces bind at razor sharp corners; the physics associated with this strong bond are not understood. Razor blades and straight pins can float on water-air surfaces pinned at the sharp corners.

Equation (4) suggests that hydrophobic nanoparticles can float on the surface no matter how heavy they are. However, even though the formula does not predict that hydrophilic particles will

sink, they will sink because of a not-understood wetting instability. If heavy nanoparticles are put into the bulk of the liquid, they will not rise. Surface tension is a property modeling rapid changes over a layer of small size which is usually taken as zero. The concept of contact angle might lose meaning if the size of the particle were smaller than the size of the layer.

I-2. Horizontal forces

The deformation of a liquid-air interface due to trapped small particles gives rise to lateral capillary forces exerted on the particle. A simple explanation is shown in figure 2. For a heavier-than-liquid particle, the meniscus is below the undisturbed level. The particles will tilt causing an imbalance of the horizontal component of capillary forces pulling the spheres together. Lighter-than-liquid hydrophilic particles will rise into the elevated section of the meniscus and come together.

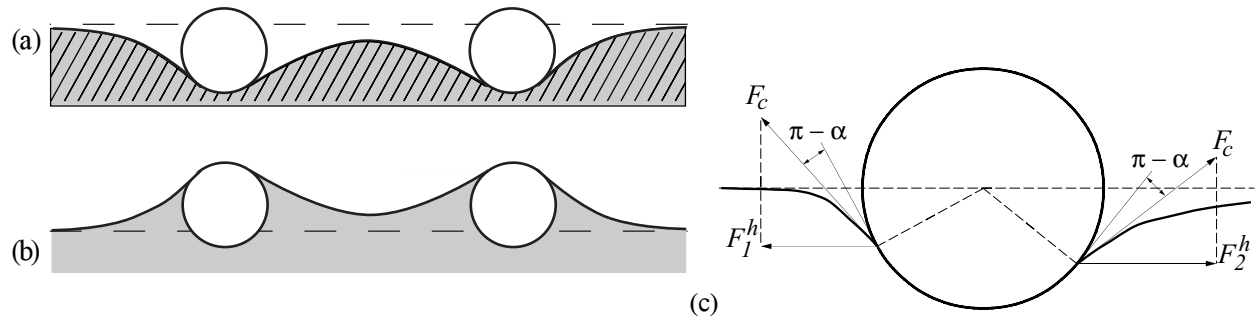


Figure 2. Spherical particles in water, (a) heavier-than-water hydrophobic particles. (b) Lighter-than-water hydrophilic particles. (c) If for any reason, the particle tilts with the two contact angles equal, a horizontal force imbalance will result. In the figure, F_c is the capillary force and F_1^h and F_2^h are horizontal components, $F_2^h > F_1^h$.

There are several ways to isolate the effects of capillarity uninfluenced by gravity. Poynting and Thompson (1913) investigated the capillary effect by considering two vertical plates immersed in a liquid, the space between the plates is a two dimensional capillary tube. If the plates are hydrophobic, the level in the capillary gap sinks below the liquid outside; if the plates are hydrophilic the level rises. Their argument about the nature of horizontal forces on the plates is given in the caption of figure 3. Repulsion between plates with different wetting properties is rather short range because it stops when the meniscus between plates gets flat.

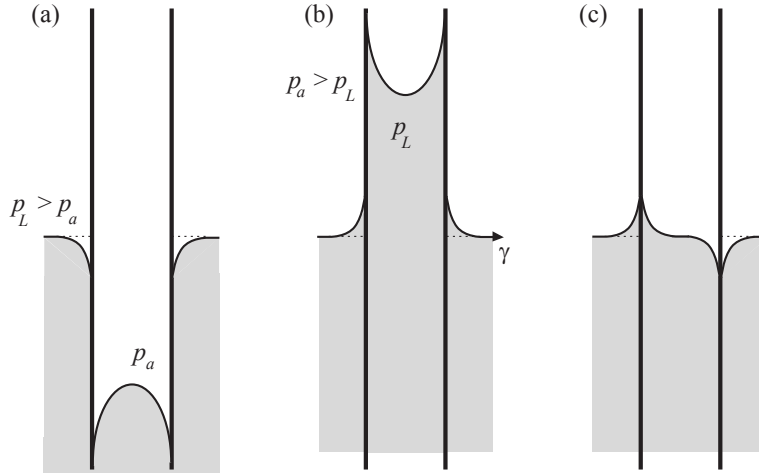


Figure 3. (After Poynting and Thompson 1913). Horizontal forces associated with the fall (a) of liquid between hydrophobic plates and the rise (b) of liquid between hydrophilic plates. In (c) one plate is hydrophilic and the other hydrophobic. The contact angles on both sides of a plate are the same and the surface tension γ is constant. They argue that the net horizontal force due to γ can be calculated at flat places; so that there is no net horizontal component of the tension. In (a) and (b) the pressures are such that they push the plates together; there is no net attractive force in (c). If the plates (c) are so close that there is no flat place, then the horizontal projection $\gamma \sin \alpha$ of the surface tension midway between the plates is smaller than the horizontal component outside the plates and the plates are pulled apart; they repel. Poynting and Thompson note that "...small bodies, such as straw or pieces of cork, floating on the surface of a liquid often attract each other in clusters; this occurs when the bodies are all wet by the liquid and also when none of them is wet; if one body is wet and one is not wet, they repel each other."

Another way to take away the effects of gravity is to support the particles on a substrate. In this case the horizontal forces are due to capillary effects alone. Katoh, Fujita and Imazu (1992) studied the motion of a particle floating on a liquid meniscus which could be interpreted as motion on a substrate because the foaming polystyrol particles used by them are an order of magnitude lighter than water, making the effects of gravity negligible compared to capillarity. Their experimental results are completely consistent with the predictions of Poynting and Thompson (1913): when the sphere and the wall are alike with respect to wetting, say both are hydrophobic or hydrophilic, the wall and sphere attract; when they are unlike the sphere and wall repel.

Despite the well-established importance of the capillary meniscus forces there are only a few theoretical works devoted to them. Nicolson (1949) was the first to derive an analytical expression for the capillary force between two floating bubbles in the linearized approximation. In this case the meniscus satisfies Laplace equation and the effects of the two bubbles on the

meniscus are simply additive. A similar approximate method was applied by Chan, Henry and White (1981) to floating spheres and horizontal cylinders. For horizontal cylinders alternative approaches were proposed by Gifford and Scriven (1971) and by Fortes (1982). The theoretical works are based on solutions of the Laplace equations for capillary menisci of translational or rotational symmetry, where the Laplace equation reduces to an ordinary differential equation.

An analytical solution of the Laplace partial differential equation in bipolar coordinates was proposed by Kralchevsky, Paunov, Ivanov and Nagayama (1992), and Kralchevsky, Paunov, Denkov, Ivanov and Nagayama (1993) for the case of small particles and small meniscus slope. This solution provides expressions for calculating the capillary meniscus force between two vertical cylinders, between two spheres partially immersed in a liquid layer and between a vertical cylinder and a sphere. A review is recently presented by Kralchevsky and K. Nagayama (2000).

Their theory (see Kralchevsky and Nagayama, 2000), which has been validated in experiments, provides the following asymptotic expression for calculating the lateral capillary force between two particles of radii R_1 and R_2 separated by a center-to-center distance L ,

$$F = -2\pi\gamma Q_1 Q_2 q K_1(qL) \left[1 + O(q^2 R_k^2) \right] \text{ when } L \gg r_k \quad (5)$$

where $r_k = R_k \sin \theta_c$ ($k=1$ and 2) are the radii of the two contact lines (see figure 1);

$$Q_k = r_k \sin \zeta_k \quad (k=1 \text{ and } 2) \quad (6)$$

with ζ_k being the meniscus slope angles with respected to the horizontal plane at the contact point ($\zeta > 0$ for floating light particles, and $\zeta < 0$ for heavy particles);

$$q = \sqrt{(\rho_l - \rho_a)g/\gamma} \quad (7)_1$$

is the inverse of the capillary length; in addition, $K_1(x)$ is the modified Bessel function of the first order. Therefore, the lateral capillary force between two identical particles is

$$F = -2\pi\gamma Q_1 Q_2 / L, \quad (7)_2$$

when the distance between them is much smaller than the capillary length ($q^{-1} = 2.7\text{mm}$ for water-air interface).

I-3. Particle clustering

Due to the attractive lateral capillary forces between similar particles floating on a liquid surface, particles tend to cluster. The dynamic behavior of clustering is not well characterized. Gifford and Scriven (1971) noted that “casual observations... show that floating needles and many other sorts of particles do indeed come together with astonishing acceleration. The unsteady flow fields that are generated challenge analysis by both experiment and theory. They will have to be understood before the common-place ‘capillary attraction’ can be more than a mere label, so far as dynamic processes are concerned.”

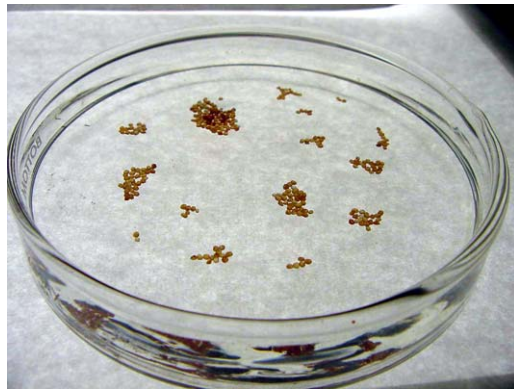
There are a small number of theoretical studies of the drag and diffusion coefficient of a spherical particle attached to a fluid interface (Brenner and Leal 1978, 1982; Goldman, Cox and Brenner 1967; Schneider, O’Neill and Brenner 1973; Majumdar, O’Neill and Brenner 1974; Wakiya 1957; Redoev, Nedjalkov and Djakovich 1992; Danov, Aust, Durst and Lange 1995). A recent study of Saif (2002) develops a theory of capillary interactions between solid plates forming menisci on the surface of a liquid.

The only experimental determination of drag coefficients for particles of any size were performed by Petkov, Denkov, Danov, Velev, Aust and Durst (1995) for particles of sub-millimeter radius by measuring the particle velocity under the action of well defined external forces. They showed that the capillary interactions are quite strong and very long range. Accelerations, which are very great under many conditions of interest, have not been studied before.

We found that the initially randomly distributed particles floating on a liquid surface tend to cluster due to the attractive lateral capillary forces between the particles. It is generally observed that the particles initially form small clusters, then the small clusters slowly merge into bigger ones; and eventually the bigger ones are assembled into a giant cluster. This self-assembly process is shown in figure 4. The procedure by which we obtain dispersions like those shown at 3 minutes in figure 4 is noteworthy. We create such dispersions by pouring particles on the liquid, nothing complicated, just like a salt shaker. As soon as the particles hit the liquid surface they disperse rapidly leading to dispersions like that at 3 minutes in figure 4. The dispersions then attract. This initial repulsion, followed by attraction, is more or less universal and we have not seen it mentioned in the literature.



Elapsed time: 3 minutes



10 minutes



30 minutes



2 hours



12 hours



24 hours

Figure 4. Free motions leading to self-assembly of floating particles. The particles are AcFrac sands with a density of 1.64 g/cm^3 and the liquid is a 1% aqueous Polyox solution with a density of 1.006 g/cm^3 (see table A1 and A2 in the appendix for more particle and liquid properties). The particles are hydrophobic and are not wetted by the aqueous Polyox solution; the capillary force not only helps the heavier-than-liquid particles float but also draws particles together.

Experiments on particle clustering due to capillarity were carried out in glass petrie dishes with diameters ranging from 5 to 15 cm. Clustering, of the type shown in figure 4, was observed

for polymer particles and nylon particles on the glycerin-air and Triton mixture-air interface. In these experiments the particles are lighter than the liquids. Properties of the particles and liquids can be found in tables A1 and A2 in the Appendix.

Rate of approach experiments were conducted for two identical nylon particles attracted by capillary forces on the glycerin-air and Triton mixture-air interface. The distance between the two particles was measured with a video camera as a function of time, as shown in figures 5 and 6. The approach of the particles takes hours, which is consistent with the time scale for cluster formation shown in figure 4. The curves in figure 5 and 6 are remarkably different at the final stage of approach, which indicates that the approach velocity depends strongly on liquid properties. Particles in a 6000 cp Triton mixture barely move even when they are placed very close together. On the other hand, the rate of approach of hydrophobic particles on water-air surfaces is surprisingly fast at the final stage of approach. The estimated final approach velocities are $0.2 \mu\text{m}/\text{s}$ and $0.025 \text{mm}/\text{s}$ for the data shown in figures 5 and 6, respectively. The approach velocity is smaller for the smaller particles, but the data was erratic and quantitative results were not obtained.

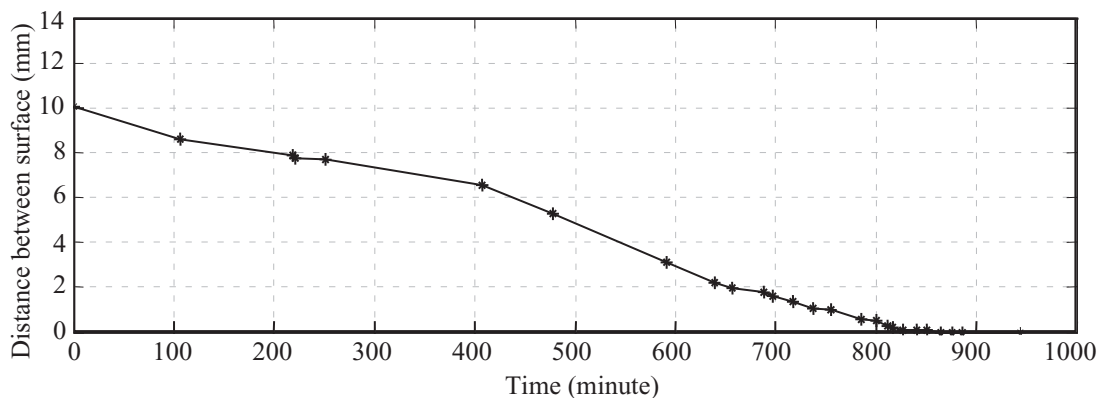


Figure 5. Distance between two identical nylon particles attracted by the capillary force on the Triton mixture (2950 cp) - air surface.

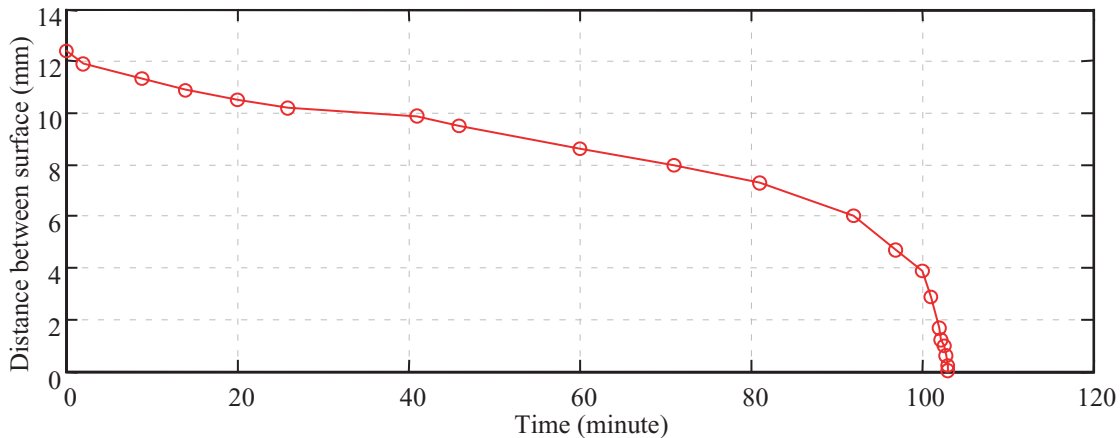


Figure 6. Distance between two identical nylon particles attracted by the capillary force on the glycerin-air interface.

Figure 7 shows the aggregation of polymer particles in a hanging glycerin film on the bottom of a flat glass plate; the photo was taken from the top of the plate. The particles are encapsulated by glycerin and drawn together in hanging drops of glycerin robustly stable for months. This hanging drop configuration is shown in figure 9 as a cartoon in side view.

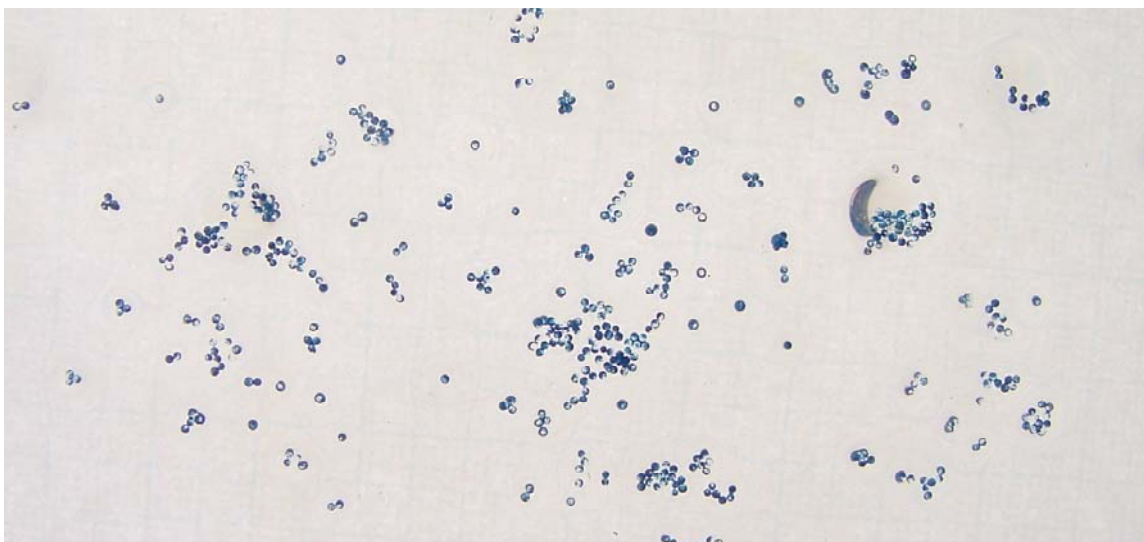


Figure 7. Aggregates of polymer particles in glycerin drops hanging from the bottom of a glass plate.

The property of self-assembly of particles by capillarity was used by Bowden *et al.* (1997, 1999) and Grzybowski *et al.* (2001) to assemble topologically complex mesoscale (from millimeter to micrometer size) objects into ordered two-dimensional arrays by floating the objects at the interface between perfluorodecalin (hydrophobic) and water. The structure of the

arrays was manipulated by the design of the shape of the assembling objects and wettability of their surfaces. They modeled the self-assembly process as the minimization of the total interfacial free energy (the sum of the capillary energy and the gravitational energy) of the liquid-liquid interface.

II. Particle aggregation in a liquid film rimming a rotating cylinder

Tirumkudulu, Tripathi and Acrivos (1999) first reported particle segregation in a suspension of monodispersed neutrally buoyant spheres in a Newtonian liquid medium being sheared in a partially filled horizontal Couette device. They found that the suspension separates itself into alternating regions of high and low particle concentration along the length of the tube. In a following study, Tirumkudulu, Mileo and Acrivos (2000) (hereafter denoted as TMA 2000) observed that under certain circumstances particles which are initially uniformly mixed in a film rimming a horizontal rotating cylinder will also be drawn into cylindrical bands of high particle concentration separated by regions of pure liquid. They did not offer a quantitative explanation of this phenomenon but suggested that the cause might be found in changes of the effective viscosity of the suspension induced by fluctuations of concentration. A theory relying on the shear induced diffusion of particles, concentration-dependent viscosity and the existence of a free surface was developed by Govindarajan, Nott and Ramaswamy (2001) to provide an explanation of the above mentioned experiments. However, quantitative comparison with the experimental data was not provided. A latest experimental result was reported by Timberlake and Morris (2002) in which concentration band dynamics was studied using a partially filled Couette device. They showed that the particle migration process observed in experiments was much faster than that predicated by the shear induced diffusion theory, about 40 times faster in one case examined, suggested strong evidence against shear-induced diffusion as the mechanism responsible for the observed segregation.

We carried out similar experiments and identified two regimes in which particles segregate; a low-speed, low-Reynolds number regime, in which particles are segregated at thin places on the rimming film by lateral capillary forces, and a high-speed regime associated with the formation of bubbles (Balmer 1970, Karweit and Corrsin 1975, Preziosi and Joseph 1988 among others). The segregation at low Reynolds numbers occurs in the parameter ranges similar to those studied by TMA 2000. The high-speed segregation has not been noted before.

II-1. The ratio of the minimum film thickness to the particle diameter

The segregation of particles due to capillarity occurs when the particles touch the interface between the film rimming the rotating cylinder and the air. The particles have the best chance to touch the interface at the thin part of the rimming film. The critical parameter for the segregation appears to be the ratio D_{min}/d_p , where D_{min} is the minimum film thickness which is near the top of the cylinder to the side in which the gravity and the vertical component of rotation point downward (figure 8). We find that D_{min}/d_p is $O(1)$ or less in all the experiments where particle segregation is observed.

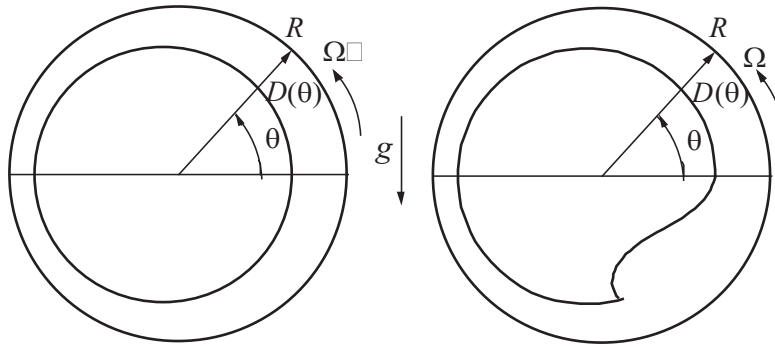


Figure 8. Film profile in rimming flow inside a rotating cylinder. (a) For small β . (b) For β larger than a critical value ($\beta_c = 1.414$).

Many authors have published analyses of lubrication flows of liquids rimming inside of a rotating cylinder: Diebler and Cerro (1970), Moffatt (1977), Preziosi and Joseph (1988), Johnson (1988), O'Brien and Gath (1998) and Tirumkudulu and Acrivos (2001). The only dimensionless parameter to arise in lubrication theory is

$$\beta = F \sqrt{\frac{gR}{\nu\Omega}} \quad (8)$$

where F is the filling level, i.e. the ratio of the total volume of liquid inside the cylinder to the volume of the cylinder; R is the radius of the cylinder; Ω is its angular rotational speed; ν is the kinetic viscosity of the liquid; g is the gravitational acceleration. The relation between β and the filling parameter F is subtle and needs clarification. When $\beta < \beta_c = 1.4142$, a smooth film exists inside the rotating cylinder. However, when β is increased beyond the critical value β_c , smooth solution of the lubrication equation does not exist, and a bump is formed near the bottom of the cylinder where the film thickness varies rapidly, as is shown in figure 8 and in figures 1 and 3 of

TMA 2000. Lubrication theory can be used to compute D_{min} when $\beta < \beta_c$; it can also be used to compute the minimum film thickness in the region above the pool of liquid when $\beta > \beta_c$ by a procedure which will be discussed below, but the solution is not valid in the liquid pool at the bottom of the cylinder. The critical condition for the existence of a smooth solution of the lubrication equation for a thin film rimming the rotating cylinder was called a “run-on” condition by Preziosi and Joseph (1988). The run-on condition was verified in experiments reported by them.

The segregation of particles by capillary forces does not correlate with β , whereas the ratio D_{min}/d_p appears to be the controlling parameter and lubrication theory can be used to compute D_{min} by the method described below. Preziosi & Joseph (1988) obtained the following equation for the thickness of the film $D(\theta)$ using a lubrication theory:

$$Q = \Omega R D - \frac{g}{\nu} \frac{1}{3} D^3 \cos \theta = \Omega R D_0 - \frac{g}{\nu} \frac{1}{3} D_0^3 \quad (9)$$

where Q is the liquid flux in the rimming flow and D_0 is the film thickness at $\theta = 0$. Let $h = D/R$ and $S = gR/\nu\Omega$, (9) can be written in the following non-dimensional form:

$$\frac{Q}{\Omega R^2} = h - \frac{1}{3} S h^3 \cos \theta = h_0 - \frac{1}{3} S h_0^3 \quad (10)$$

where $h_0 = h(\theta)$ at $\theta = 0$ and it is the maximum non-dimensional film thickness (see figure 8). Preziosi & Joseph gave the condition under which equation (10) is solvable,

$$h_0^2 S < 1, \quad (11)$$

which is the run-on condition.

O'Brien and Gath (1998) defined $\eta = D \left(\frac{g}{\Omega R \nu} \right)^{1/2} = \frac{D}{R} S^{1/2}$ and $q = Q \left(\frac{g}{\Omega^3 R^3 \nu} \right)^{1/2} = \frac{Q}{\Omega R^2} S^{1/2}$

and wrote

$$q = \eta - \frac{1}{3} \eta^3 \cos \theta = \eta_0 - \frac{1}{3} \eta_0^3. \quad (12)$$

They gave the condition under which equation (12) is solvable:

$$0 < q < 2/3. \quad (13)$$

Note that when $q = 2/3$, the solution of (12) is $\eta_0 = h_0 S^{1/2} = 1$. Hence, the run-on criterion (11) is equivalent to (13).

The fluid fraction F can be computed by integrating $D(\theta)$:

$$F = \frac{1}{\pi R} \int_{-\pi}^{\pi} D(\theta) d\theta \equiv \frac{\beta}{S^{1/2}}, \text{ where } \beta = \frac{1}{\pi} \int_{-\pi}^{\pi} \eta(\theta) d\theta. \quad (14)$$

By virtue of (12) and (14), the value of β corresponding to $q = 2/3$ is $\beta = 1.4142$. Therefore, the three critical conditions for the existence of a smooth solution of the lubrication equation are equivalent: $h_0^2 S < 1$, $0 < q < 2/3$, and $\beta < 1.4142$.

When $\beta < 1.4142$, all the liquid is in the thin film without a bump; the liquid flux can be obtained from F ,

$$\frac{Q}{\Omega R^2} = \frac{F}{2}. \quad (15)$$

Then equation (10) can be solved for the non-dimensional film thickness profile $h(\theta)$,

$$h - \frac{1}{3} S h^3 \cos \theta = \frac{1}{2} F, \quad (16)$$

and the minimum film thickness can be obtained at $\theta = \pi$.

The maximum non-dimensional film thickness h_0 at $\theta = 0$ is an increasing function of β with a maximum at $\beta = \beta_c$. When $\beta > \beta_c = 1.4142$, there are places on the cylinder where the thickness of the layer is larger than the critical value, and the excess liquid will collect under the bump. However, it may be assumed that h_0 remains at $\theta = 0$ (see figure 8); it is the maximum thickness of the film above the bump. This assumption could not be strictly correct; Ruschak and Scriven (1976) showed that under a perturbation of the thin film condition used to justify lubrication theory, the position of the maximum thickness rotates into the first quadrant. We assume that the maximum film thickness that can be maintained by rotation is determined by the run-on condition (11): $h_0 = 1/\sqrt{S} = \sqrt{\nu \Omega / g R}$. Then we can calculate the actual liquid flux in the circulation by

$$\frac{Q}{\Omega R^2} = h_0 - \frac{S}{3} h_0^3 = \frac{2}{3\sqrt{S}}. \quad (17)$$

The minimum film thickness at $\theta = \pi$ is determined from the volume conservation (10),

$$\frac{Q}{\Omega R^2} = h_{\min} + \frac{S}{3} h_{\min}^3 = \frac{2}{3\sqrt{S}}$$

or,

$$h_{\min} = \frac{0.596}{\sqrt{S}} = 0.596 \sqrt{\frac{\nu\Omega}{gR}}. \quad (18)$$

Tirumkudulu & Acrivos (2001) solved for the film profile using an extended lubrication analysis and numerical computation from the full Stokes equations, and compared their solutions with experimental measurements. Their results (their figures 3-5) show that the value of $\eta_{\min} = h_{\min} \sqrt{gR/(\nu\Omega)}$ is at about 0.6, which is in excellent agreement with our expression (18) based on a much simpler argument. When β is greater than β_c , the minimum film thickness D_{\min} listed in table 1 are evaluated from (18). We may also calculate the average film thickness D_a from

$$F = \frac{R^2 - (R - D_a)^2}{R^2}, \text{ i.e. } D_a = (1 - \sqrt{1 - F})R. \quad (19)$$

II-2. Particle segregation in aqueous Triton mixtures

TMA 2000 found particle segregation in monodispersed sheared suspensions in a partially filled rotating horizontal cylinder when the filling fractions were small ($0.1 \leq F \leq 0.15$). The particle concentrations for the uniform mixtures were 5% and 15%. The values of β in experiments reported in TMA 2000 were all greater than β_c .

Systematic experiments on clustering of particles into bands were carried out using the polymer particles whose properties can be found in table A2. The liquids used in these experiments are mixtures of Triton X 100, ZnCl_2 and water, which are the same kind of liquids as used in TMA 2000. The mixtures have viscosities in the range of 2-60 poise and densities in the range of 1.1-1.5 g/cm^3 , depending on the fractions of the components. The viscosities of the mixtures are sensitive to the temperature which was maintained at $68 \pm 2^\circ\text{F}$ in our experiments.

The experiments were conducted in two cylinders, one is 30 cm long with a inner diameter of 2.792 cm; the other is 15 cm long with the same inner diameter. The cylinder is supported horizontally and is driven at constant rotational speed Ω by a motor. The Reynolds number

$R_e = (\Omega D_a^2)/\nu$ in these experiments is very small (less than 10^{-2}), hence inertial effects are negligible.

	F	R (cm)	Ω (rpm)	μ (poise)	ρ (g/cm ³)	ν (cm ² /s)	β	D_a (cm)	D_{min} (cm)	D_{min}/d_p
TMA 1	0.150	1.270	1.40	40.00	1.172	34.13	2.36	0.099	0.0480	1.04
TMA 2	0.125	5.000	2.80	49.00	1.172	41.81	2.50	0.323	0.149	3.24
M1	0.151	1.396	1.65	51.95	1.241	41.86	2.08	0.110	0.0605	0.931
M2	0.140	1.396	1.65	29.50	1.332	22.15	2.05	0.101	0.0440	0.677
M3	0.150	1.396	1.10	51.95	1.241	41.86	2.53	0.110	0.0494	0.760
M4	0.145	1.396	10.9	48.50	1.212	40.02	0.79	0.105	0.0966	1.49
M5	0.061	1.396	1.76	44.34	1.203	36.86	0.87	0.043	0.0403	0.620
M6	0.061	1.396	3.13	44.34	1.203	36.86	0.65	0.043	0.0412	0.634
M7	0.061	1.396	6.00	44.34	1.203	36.86	0.47	0.043	0.0418	0.648
M8	0.061	1.396	10.0	44.34	1.203	36.86	0.37	0.043	0.042	0.646
M9	0.046	1.396	38.71	2.377	1.498	1.587	0.67	0.032	0.0310	0.477
M10	0.046	1.396	51.10	2.377	1.498	1.587	0.58	0.032	0.0313	0.482

Table 1. Parameters for experiments reported in TMA 2000 and for our experiments (M1 through M10). Experiments M4 and M5 were conducted in the 15-cm-long cylinder; the other experiments were conducted in the 30-cm-long cylinder.

In table 1 we list the parameters for the experiments using Triton mixtures reported in TMA 2000 and our experiments M1 through M10. The derived parameters ($\beta, D_a, D_{min}, D_{min}/d_p$) are based on the properties of the pure liquids. The particles used in TMA1 and TMA2 were neutrally buoyant with density 1.172 g/cm^3 , and diameter $d_p = 0.04625 \pm 0.00375 \text{ cm}$ in concentrations of 15%. The values of β for TMA1 and TMA2 based on the viscosity of the homogenous suspension would be 1.8 and 1.9, respectively. In our experiments M1 through M10, the particle density $\rho_p = 1.034 \text{ g/cm}^3$ is smaller than the liquid density; the diameters of the particles are more dispersed with an average particle diameter $d_p = 0.065 \text{ cm}$. The concentrations of the particles range from 2% to 7%. Although our particles are not neutrally buoyant, the sedimentation of the particles in the liquids used in the experiments can be neglected, since the sedimentation velocity of the particles in those liquids is of the order of 10 nm/s .

Particle segregation was observed in all the experiments listed in table 1 and we note that the values of D_{\min}/d_p in table 1 are all of $O(1)$ or less. In the experiments M1, M2 and M3, the value of β is larger than β_c and a pool of liquid exists at the bottom of the rotating cylinder. The capillary attraction forces act mainly at the top part of the cylinder where particles touch the surface of the thin film. The rotational speed of the cylinder must be slow enough relative to the speed of capillary attraction to allow clusters to form at the top more rapidly than they disperse in the pool of liquid at the bottom. In the experiments M4 through M10, β is smaller than β_c and the film is smooth around the cylinder. The film thickness is smaller than or close to the particle diameter and the capillary attraction force can draw particles into clusters even when the rotational speed is relatively high (51.1 rpm in M10). We do not know the reason of particle segregation in TMA 1 and 2, however, capillarity may play a role there too.

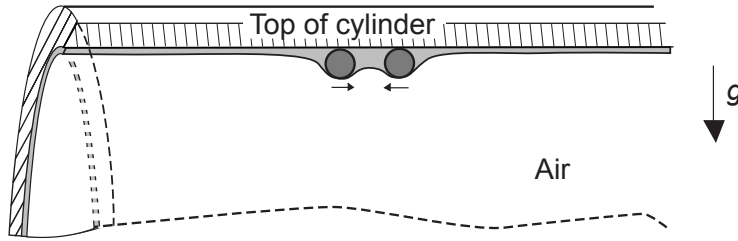


Figure 9. Capillary attraction of two particles hanging in a film at the top of a stationary rotating cylinder. The liquid film is the top section (the gray area). The air fills the other space.

After the cylinder is partially filled with the uniform suspension, it is turned a few times by hand and then put to rest so that the suspension covers the whole inside cylinder. It is observed that particles trapped in the thin film at the top of the cylinder move rather rapidly together under the action of capillarity (see figure 9). A similar kind of dynamics prevails when the cylinder rotates continuously at a constant velocity. In general the trapped particles are completely wetted by the liquid as they go round and round with the rotating cylinder. The segregation of particles generally occurs slowly and it takes a long time (hours) for the particles to reach the final steady band formation. The process of particle segregation can be divided into several stages. The first is the formation of many small particle clusters, which are nucleated randomly along the cylinder a few minutes after the beginning of rotation. Small particle clusters merge into larger ones as time goes by. Then clusters form several large and rather stable blocks which are often far from each other. The blocks are gradually stretched thinner and longer in the flow direction, and eventually form cylindrical bands. The final formation of the bands is frequently uniform along

the cylinder axis. The bands are not robustly stable; they may form, move, break, reform or merge. It can be said that uniform dispersion is robustly unstable and clusters are robustly stable. The snap shots of the particle band formation are shown in figure 10.



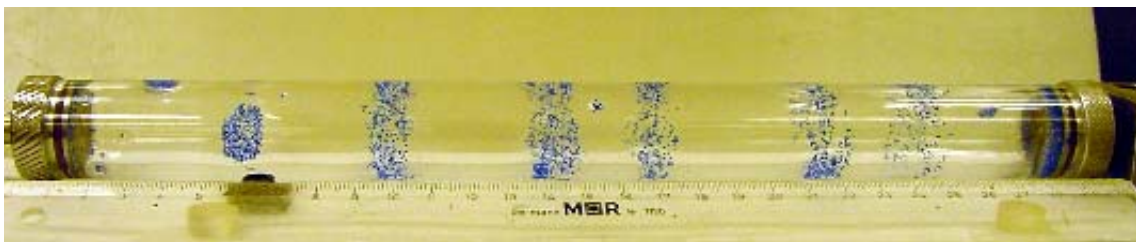
(a) Uniform distribution of particles at the beginning



(b) Particle clusters



(c) Larger clusters



(d) Particle bands

Figure 10. Stages of particle band formation. The experiment was performed in a highly viscous Triton mixture at a low rotational speed with a low filling level (M7 in table 1).

In table 2, we list the values for the times of formation of small clusters t_{w1} , large clusters (called blocks) t_{w2} and bands t_{w3} and the distance between bands as a function of the filling level and rotational speed. It appears that bands form faster when the rotational speed is increased at the same filling level.

Filling level F	Rotational speed Ω (rpm)	Waiting time for particle clusters t_{w1} (hour)	Waiting time for large blocks t_{w2} (hour)	Waiting time for bands t_{w3} (hour)	Average distance between bands \bar{l} (cm)
0.061	1.76	1.1	2.6	6.6	6.2
0.061	3.13	0.8	2.1	4.7	5.5
0.061	6.00	0.6	2.2	4.0	3.9
0.061	10.0	0.5	1.8	3.5	4.5
0.046	38.71	0.10	0.25	0.40	3.9
0.046	51.10	0.08	0.20	0.30	3.6

Table 2. Times for cluster and band formation and average distance between bands (the data are for experiments M5-M10 in table 1).

Particle band formation is observed in the Triton mixtures with viscosities as high as 52 poise and as low as 2.38 poise (see table 1). Relatively low filling levels and high rotational speeds are needed to achieve band formation in the low-viscosity Triton mixture (M9 and M10). The stages of particle segregation in the low-viscosity Triton mixture (shown in figure 11) are similar to those in high-viscosity Triton mixtures (figure 10). However, the rotational speed cannot be too high, otherwise particle bands do not form or they may form but are not stable. We did experiments with soybean oil and glycerin at relatively high rotational speeds (the corresponding values of β are 1.0 - 1.2) and did not observe particle bands; however, particle clusters were always generated by capillary induced “anti-diffusion”.

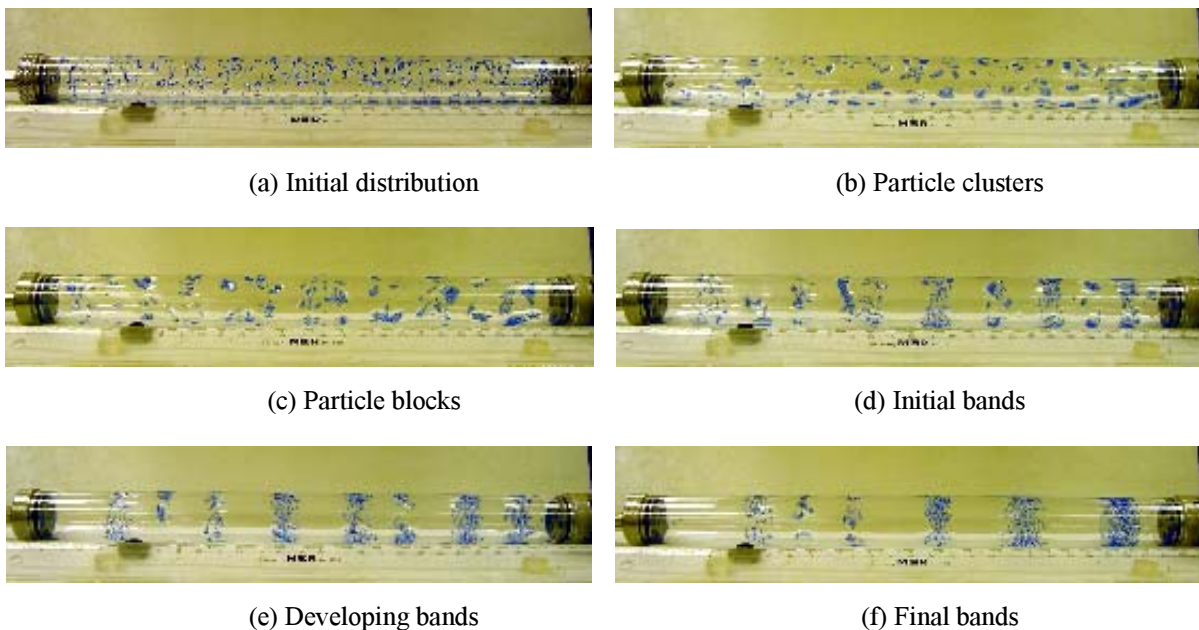


Figure 11. Stages of particle band formation. The experiment was performed in a low-viscosity Triton mixture at a relatively high rotational speed with a low filling level (M10 in table 1).

The configurations of the bands are different in high filling level experiments and low filling level experiments. In high filling level experiments, there are many particles in the liquid sections between particle bands (see figure 12) and weak secondary flow and transverse movement of particles can be seen between particle bands. In contrast, in the low filling level experiments clear pure liquid between the particle bands is observed (see figures 10d and 11f).

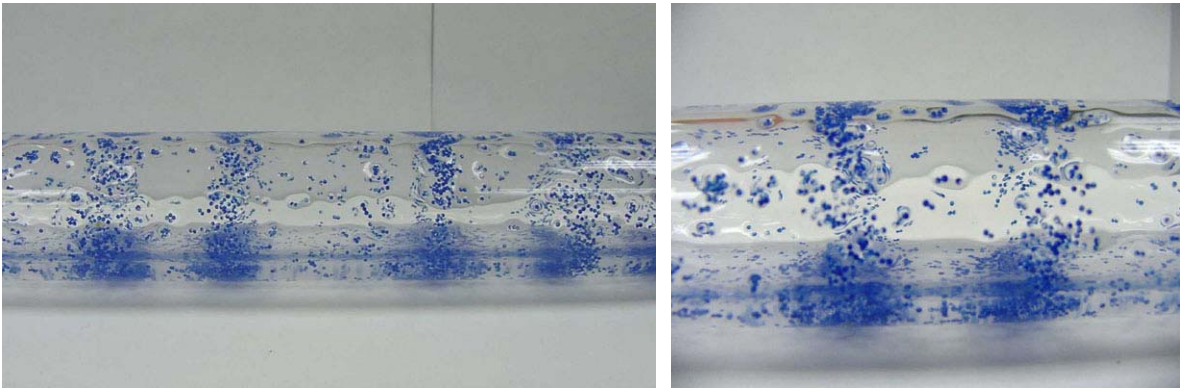
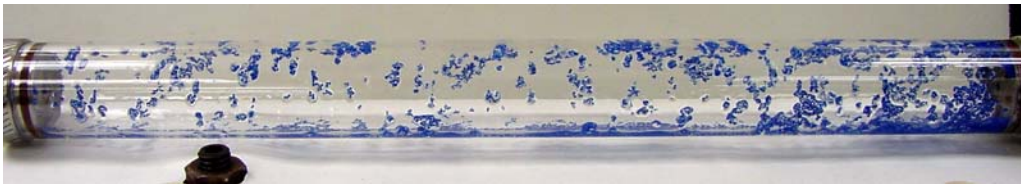


Figure 12. Particles which are initially distributed uniformly in a film rimming a rotating cylinder segregate into cylindrical bands (M3 in table 1). The formation of the bands takes hours.

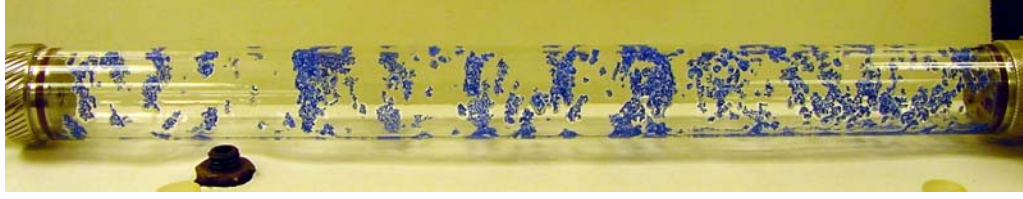
In this section we described cluster and band formation due to capillarity for lighter-than-liquid polymer particles in small concentrations in a highly viscous Triton mixture under conditions in which $D_{min}/d_p = O(1)$.

II-3. Particle segregation in water

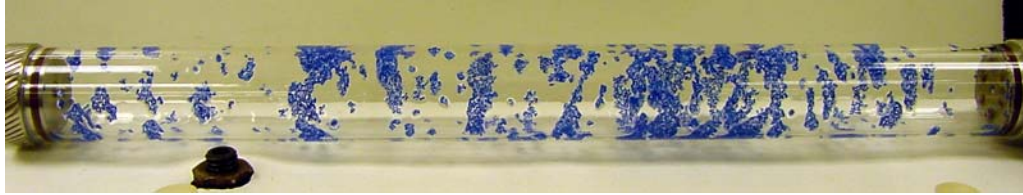
Particle segregation is observed in water using the polymer particles. In figure 13 we show cluster and band formation due to capillarity in large concentration 20.7% with $\beta = 15.94$.



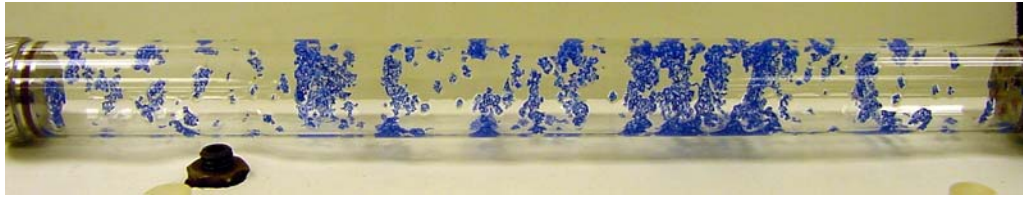
(a) 3 minutes after the beginning of rotation.



(b) 1.5 hours after the beginning of rotation.



(c) 6 hours after the beginning of rotation.



(d) 18 hours after the beginning of rotation.

Figure 13. Band formation of particles due to capillarity. The liquid is water (18°C) and the particles are polymer particles. The filling level F is 0.041 and the particle concentration is 20.7%. The rotational speed $\Omega = 8.57$ rpm, $\beta = 15.94$, average film thickness $D_a = 0.288$ mm, minimum film thickness $D_{min} = 0.0213$ mm, $D_{min}/d_p = 0.033$.

II-4. Particle segregation in glycerin

Cluster and band formation due to capillarity is very robust in thin films on the inside of a rotating cylinder. In figures 14, 15 and 16 we show clusters and bands in glycerin using almost neutrally buoyant particles, heavier-than-glycerin particles and lighter-than-glycerin particles, respectively. Particle concentration varies from 4.8% to 54.2% and particle diameter varies from 0.065cm to 0.314cm.



Figure 14. Clustering of particles due to capillarity. The liquid is glycerin with a density of 1.173 g/cm³, and the particles are nylon particles with a density of 1.170 g/cm³ and a diameter of 0.314cm. The

filling level F is 0.082 and the particle concentration is 54.2%. The rotational speed $\Omega=5.45$ rpm, $\beta=1.127$, average film thickness $D_a=0.585$ mm, minimum film thickness $D_{min}=0.526$ mm, $D_{min}/d_p=0.176$. Clusters of particles form about 5 minutes after the beginning of rotation. Bands form occasionally but are not stable.



(a) 2.5 hours after the beginning of rotation.



(b) 16 hours after the beginning of rotation.

Figure 15. Band formation of particles due to capillarity. The liquid is glycerin with a density of 1.173 g/cm³, and the particles are 16/20 Naplite sands with a density of 2.59 g/cm³ and a diameter of 0.959 mm. The filling level F is 0.0785 and the particle concentration is 13.0%. The rotational speed $\Omega=5.45$ rpm, $\beta=1.079$, average film thickness $D_a=0.559$ mm, minimum film thickness $D_{min}=0.506$ mm, $D_{min}/d_p=0.528$.



Figure 16. Band formation of particles due to capillarity. The liquid is glycerin with a density of 1.173 g/cm³, and the particles are polymer particles with a density of 1.034 g/cm³ and a diameter of 0.65 mm. The filling level F is 0.105 and the particle concentration is 4.8%. The rotational speed $\Omega=5.45$ rpm, $\beta=1.443$, average film thickness $D_a=0.753$ mm, minimum film thickness $D_{min}=0.605$ mm, $D_{min}/d_p=0.931$. Band formation 15 hours after the beginning of rotation is shown in the figure.

III. Particle segregation due to the formation of bubbles

When a partially filled horizontal cylinder rotates at moderate speeds and the effects of surface tension and gravity are both important, air bubbles separated by disks of liquid will form. The bubbles are then not centered and can take different shapes depending on relevant parameters. The off-center bubbles pump the liquid to form the secondary motion which is from

the bubble to the liquid disks near the bubble surface and from the liquid disks to the bubble near the wall (see figure 19). Particles are centrifuged to the wall if they are heavier than the liquid, centrifuged to the surface of the bubble if they are heavier than the air but lighter than the liquid. Driven by the secondary motion, lighter-than-liquid particles aggregate in the liquid disks; heavier-than-liquid particles aggregate in the region circling the bubbles when the bubbles are off the wall, and in the liquid disks when the bubbles touch the wall.

III-1. Bubbles in a partially filled rotating cylinder

If the filling fraction is not small in the rimming flow inside a partially filled rotating horizontal cylinder, air bubbles will form and the shape, number and position of these bubbles depend on F , the rotational speed Ω , the surface tension γ , the viscosity of the liquid, the density difference between liquid and gas $\rho_l - \rho_g$, and the dimensions of the apparatus. The qualitative effects of all these parameters are fairly well understood.

When the cylinder rotates so fast that the effects of the centrifugal gravity $\Omega^2 R$ overwhelm those of terrestrial gravity, i.e. $\Omega^2 R/g \gg 1$, all of the liquid is centrifuged and rotates with the cylinder as a rigid body. In this case the air is centered and if the filling level is large enough (in our experiments $F \geq 0.5$), bubbles will form under the action of an interfacial potential (see Preziosi and Joseph 1987). An important parameter for this potential is

$$J = \frac{(\rho_l - \rho_g)\Omega^2 R_b^3}{\gamma} \quad (20)$$

where R_b is the maximum radius of the bubble. J does not depend on gravity, viscosity, filling level or the length of the apparatus. If $J < 4$ cigar shaped bubbles will form; the bubbles are all identical but the number of them depends on the filling level and the history of their creation. $J = 4$ is a limiting value restricting the bubble parameters; when Ω is increased, the maximum radius of the bubble decreases in such a way that $J = 4$; when the ratio of bubble length to radius $L/R_b > 8$, the bubble shape is very closely approximated by a cylinder of constant radius R_b bounded by two semi-spherical end caps (this is achieved in figures 17g, h).

The condition $J = 4$ was derived from heuristic arguments by Vonnegut (1942). It is the working formula for the “spinning drop” tensiometer which is used to measure interfacial tension (see Joseph *et al.* 1992).

As Ω is increased, R_b decreases with $J = 4$. Since the bubble volume is fixed the length L increases and eventually all the bubbles collect end to end to form a long, rigorously centered, cylindrical column, which does not change under further increases of angular velocity.

Coming the other way, as Ω is decreased from a state where $\Omega^2 R/g \gg 1$, the length of the bubbles will decrease and the maximum radius R_b will increase with $J = 4$. When $\Omega^2 R/g \sim O(1)$, the effect of terrestrial gravity becomes important and the bubbles rise; secondary motions are generated and the rotational speed becomes important. Photographs which exhibit typical configurations of bubbles are displayed in figure 17 where the soybean oil with a viscosity of 282 cp is compared to the Triton mixture with a viscosity of 2950 cp. The main effect of viscosity here is to maintain the rigid rotational motion of the liquid subject to perturbations of gravity. The cylinder used in the experiments in section III has an inner diameter of 1.28 cm and a length of 22.14 cm. The ratios of centrifugal to terrestrial gravity at several rotational speeds are listed below:

Ω	200	300	600	1000
$\Omega^2 R/g$	0.287	0.64	2.57	7.16

Table 3. Gravity ratios at several rotational speeds.

At high rotational speeds ($\Omega = 900$ or 1000 rpm), the bubbles are rigorously centered in both the soybean oil and the Triton mixture (see figures 17g and 17h). Such configurations of centered bubbles, whose shape is determined by a potential lined up end to end, are essentially uninfluenced by gravity. The effects of gravity become sensible at $\Omega = 600$ rpm and the configurations of bubbles in the soybean oil and in the Triton mixture are different. The perturbation of the rigid rotational motion in the high viscosity Triton mixture is small and the secondary motions are much weaker than in the soybean oil. The distortion of the bubbles is more severe in the soybean oil than in the Triton mixture. At even lower values of Ω , the air in the soybean oil forms a single bubble which rises to the top, whereas bubbles still exist in the Triton mixture although heavily distorted by gravity.



(a) Soybean oil, $\Omega = 200$ rpm



(b) Triton mixture, $\Omega = 200$ rpm



(c) Soybean oil, $\Omega = 300$ rpm



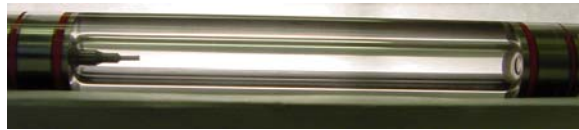
(d) Triton mixture, $\Omega = 300$ rpm



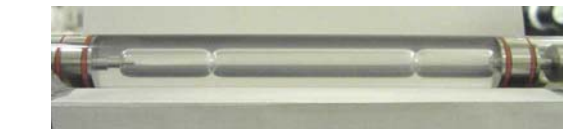
(e) Soybean oil, $\Omega = 600$ rpm



(f) Triton mixture, $\Omega = 600$ rpm



(g) Soybean oil, $\Omega = 1000$ rpm



(h) Triton mixture, $\Omega = 900$ rpm

Figure 17. Comparison of bubble formation in the soybean oil and the Triton mixture (2950 cp).

As the rotational speed is decreased to zero, the liquid and air stratify with all the air at the top. Even in this case, a stationary liquid, the air may separate into bubbles induced by capillarity if the amount of the air is not small; if the filling level is near one, the very small amount of air will rise to the top and form a single short bubble due to the restraining action of surface tension.

Many unusual shapes of bubbles may occur when $\Omega^2 R/g \sim O(1)$, as put into evidence and in the papers by Balmer (1970), Sanders, Joseph and Beavers (1981) and Preziosi and Joseph (1988).

The combined effects of the filling level and rotational speed on the formation of the bubbles are of interest. When the gravity ratio parameter is small, $\Omega^2 R/g \ll 1$, the liquid and air are stratified with a thin film being dragged up by the rotating cylinder. If the filling level is large enough, the thickness of the film dragged up increases as the cylinder rotates faster. Up to a critical condition, the thick liquid film on the top of the cylinder cannot be maintained and part of it falls down under gravity, subsequently the single air bubble breaks. On the other hand, when the gravity ratio parameter is large, the air forms a rigorously centered cylindrical column

stretching from end to end of the cylinder. If the rotational speed decreases, the stabilizing effect of the centrifugal acceleration decreases. Up to a point, the combined effects of the surface capillarity and the terrestrial gravity will break up the air bubble into smaller ones.

The critical conditions under which the single air bubble breaks were determined experimentally for the rimming flow of soybean oil. The two lines on the (F, Ω) plane in figure 18 indicate the critical conditions. When the filling level and rotational speed fall in the region between the two lines, separated bubbles are observed; otherwise, a single air bubble is stable. Note that when $F < 0.4$, a single air bubble is stable at any rotational speed.

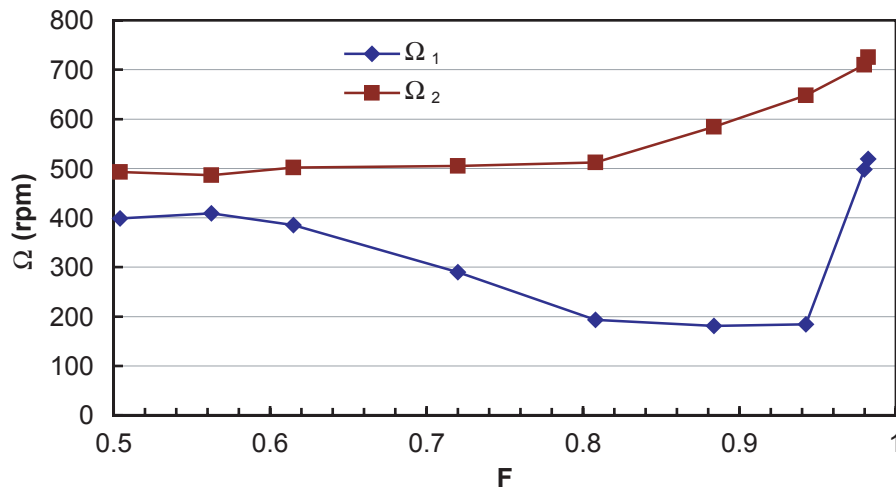


Figure 18. Critical conditions for the formation of bubbles in soybean oil. The experiments were carried out in a glass cylinder with an inner diameter of 1.28 cm and a length of 22.14 cm. When $F < 0.4$, a single air bubble is stable at any rotational speed. For $F \geq 0.5$, when the rotational speed is between Ω_1 and Ω_2 , separated bubbles are observed.

III-2. Particles segregation due to bubbles

In a system with several air bubbles distributed along the length of the cylinder and displaced off the axis of the rotation by the action of gravity, the motion of the particles suspended in the liquid may be driven by the secondary motions associated with the pumping effect around the off-center bubbles. The off-center bubbles are stationary and act as obstacles around which the liquid must pass. The pumping motion of the bubble sets up an eddy which will push the liquid from the bubble to the liquid disks near the bubble surface and from the liquid disks to the bubble near the wall (see figure 19).

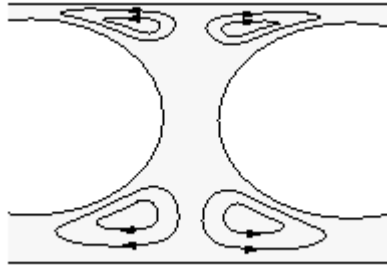
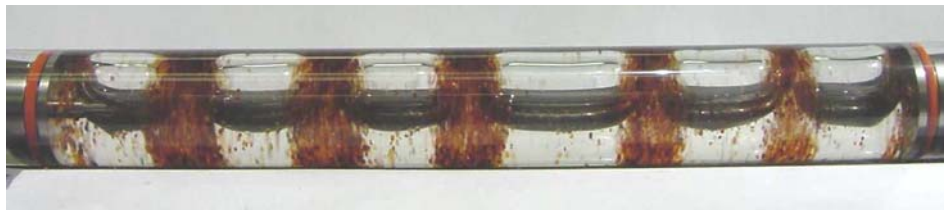


Figure 19. The eddies set up by the pumping motion of the off-center bubbles. Liquid flows from the bubble to the liquid disks near the bubble surface and from the liquid disks to the bubble near the wall.



(a) $\Omega = 200$ rpm



(b) $\Omega = 300$ rpm



(c) $\Omega = 600$ rpm



(d) $\Omega = 1000$ rpm

Figure 20. Particle segregation of resin particles with $\rho_p = 1.13 \text{ g/cm}^3$ in the soybean oil with $\rho_l = 0.915 \text{ g/cm}^3$. The particle concentration is 15% and the filling level $F=0.6$.

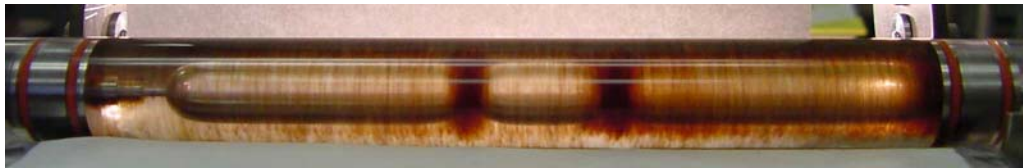
The changes in the nature of heavier-than-liquid particle segregation as $\Omega^2 R/g$ changes (see table 3) are shown in four panels of figure 20 where we go from stratified flow (a) to uniform flow (d). Comparing figures 17(a, c) with figures 20(a, b) we see that the particles promote

bubbles formation at low rotational speeds in soybean oil. This effect may be due to the increase in the effective density of the mixture which increases the value of J in (20) by replacing ρ_l with $\rho_c = \rho_p\phi + \rho_l(1 - \phi)$ where ϕ is the particle fraction.

The heavier-than-liquid particles are centrifuged to regions near the cylinder wall where secondary motions are weakest. The eddies push the particles on the wall to the region circling the bubbles and away from the liquid disks when the rotational speed of the cylinder is large enough to centrifuge the air away from the wall but not so large as to center it (figure 20c). At lower speeds, the bubbles rise all the way to the wall and the particles on the wall are pushed to the liquid disks (figures 20a,b).



(a) 200 rpm



(b) 600 rpm

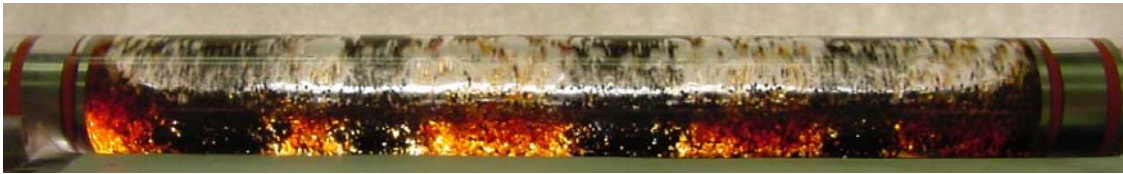
Figure 21. Particle segregation of resin particles with $\rho_p = 1.13 \text{ g/cm}^3$ in glycerin with $\rho_l = 1.173 \text{ g/cm}^3$. The particle concentration is 8.96% and the filling level $F=0.667$.

Figure 21 shows the segregation pattern of lighter-than-liquid particles. The lighter-than-liquid particles are centrifuged to the surface of the bubbles and pushed to the liquid disks by the eddies described in figure 19. In figure 21(b), some particles do circulate around the bubbles because the bubbles are almost centered and the secondary motions are weak. At 600 rpm, heavier-than-liquid particles are centrifuged to the wall and aggregate above the bubbles as shown in figure 20(c) whilst lighter-than-liquid particles are centrifuged to the surface of the bubbles and aggregate in the liquid disks as shown in figure 21(b).

III-3. Segregation of bi-disperse suspension in a partially filled rotating cylinder

Preliminary experiments using suspensions of particles with two different densities show that the rotating flow leads to segregation of the two types of particles into separate regions whose exact form depends on the density and concentration of particles and on other features which have yet to be determined. Here we show that this kind of segregation does occur and is robust.

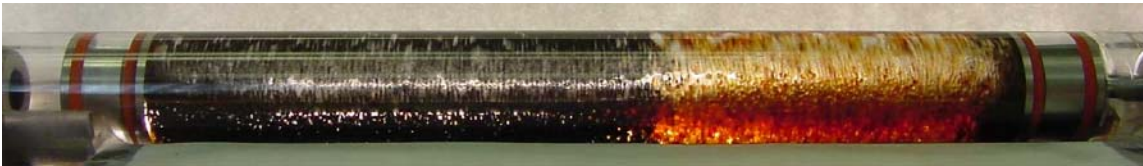
Figure 22 and 23 show two experiments of segregation of bi-disperse suspension in aqueous glycerin solutions. The different concentrations of the particles cause different patterns of segregation (figure 22a and figure 23a). The rotating flow finally leads to uniform distribution of the particles, with the heavy particles at the end of the cylinder and the light particles at the middle of the cylinder (figure 22c and figure 23c). Figure 24 shows bi-disperse suspension in water. The configuration shown in figure 24 is stable for hours. The two types of particles used in these experiments are black silicon particles with $\rho_p = 3.07 \text{ g/cm}^3$ and an average diameter $d_p = 0.05 \text{ cm}$, and brown resin particles with $\rho_p = 1.13 \text{ g/cm}^3$ and an average diameter $d_p = 0.065 \text{ cm}$.



(a) 30 minutes after the beginning of rotation.

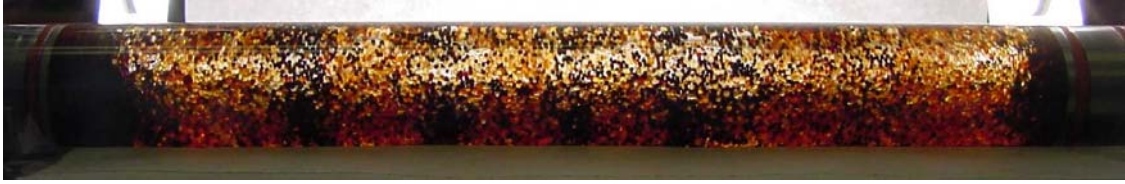


(b) two hours after the beginning of rotation.

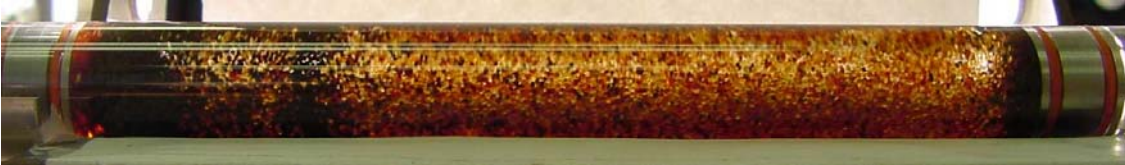


(c) 20 hours after the beginning of rotation.

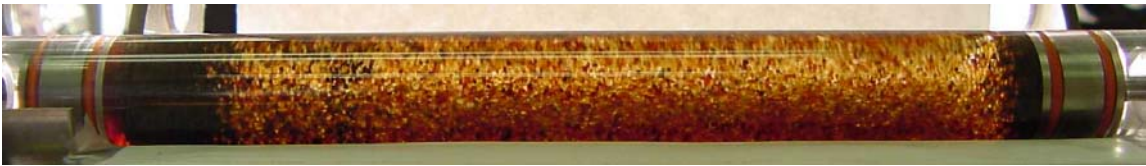
Figure 22. Segregation of two types of particles in a 47.8% aqueous glycerin solution with $\rho_l = 1.09 \text{ g/cm}^3$. The filling level $F=0.354$. The concentrations of the black silicon particles and brown resin particles are 21.7% and 12%, respectively. The rotational speed is 165 rpm.



(a) Four minutes after the beginning of rotation.



(b) 24 minutes after the beginning of rotation.



(c) 36 minutes after the beginning of rotation.

Figure 23. Segregation of two types of particles in a 48.7% aqueous glycerin solution. The filling level $F=0.328$. The concentrations of the black silicon particles and brown resin particles are both 16%. The rotational speed is 160 rpm.

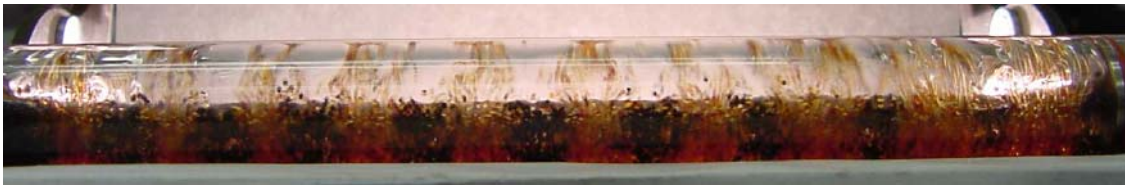


Figure 24. Segregation of two types of particles in water. The filling level $F=0.357$. The concentrations of the black silicon particles and brown resin particles are 4% and 16%, respectively. The rotational speed is 306 rpm.

IV. Conclusion

The principal facts concerning capillary attraction and self-assembly of small lighter- and heavier-than-fluid floating particles were reviewed. These facts were applied to explain the clustering and segregation of bands of particles in a thin liquid film rimming the inside of a partially filled, slowly rotating cylinder in situations resembling those first observed by Tirumkudulu, Mileo and Acrivos (2000). In our experiments clustering and band formation occurred under all kinds of conditions, for liquids with high and low viscosities, for particles lighter- and heavier-than-liquids, for small particles and large particles, and for low

concentrations and high concentrations of particles. Uniform dispersions of particles in thin films are robustly unstable to anti-diffusion due to capillarity, and clusters which are self-assembled are robustly stable. The conditions required to support this phenomenon are that the liquid film is thin relative to the particle size; the film should be thin, or in any case, not much thicker than the particles. The rotational speed of the cylinder should be slow enough that the time needed for sensible capillary attraction is comparable to the time of residence of the particle in the thin part of the rimming film.

Particle segregation may also be generated by pumping secondary motions of fluid by off-center gas bubbles, which arise when the gravity parameter $\Omega^2 R/g \sim O(1)$ and the filling level is not too small. Lighter-than-liquid particles segregate in the liquid disks between bubbles; heavier-than-liquid particles segregate in the region above the bubbles when they are off the wall, and in the liquid disks when the bubbles touch the wall.

A third regime of segregation of bi-disperse suspension of particles of different heavier-than-liquid densities, which stratify when the cylinder is at rest, form into rings when the cylinder rotates. Different forms of the ring appear to depend on the particle concentration and other factors which have as yet to be determined.

Appendix

The properties of the liquids and particles used in the experiments reported here are listed in the following tables.

type of liquid	glycerin	soybean oil	1% aqueous Polyox	water	Triton mixture		
					sample 1	sample 2	sample 3
density ρ_1 (g/cm ³)	1.173	0.915	1.006	1	1.241	1.203	1.498
viscosity μ (cp)	1490	282	7650	1	2950	4434	238
surface tension (mN/m)	41.46	24.28	56.89	67.36	33.15	32.36	37.28

Table A1. Material parameters for liquids used in the experiments. The viscosity of 1% aqueous Polyox solution listed here is zero shear viscosity. The values of surface tension are measured using a spinning-drop tensiometer. The Triton mixtures are combinations of Triton X 100, ZnCl₂ and water. The mixtures we prepared have viscosities in the range of 2 – 60 poise and densities in the range of 1.1 - 1.5 g/cm³, depending on the fractions of the components. Three samples of them are listed here.

type of particle	polymer particle	nylon particle	16/30 AcFrac PR sand	16/20 Naplite sand	resin particle	silicon particle
density ρ_p (g/cm ³)	1.034	1.170	1.640	2.59	1.13	3.07
average diameter d_p (cm)	0.065	0.314	0.088	0.959	0.065	0.05

Table 2. Physical parameters for particles used in the experiments.

Acknowledgement

The work of authors Joseph, Wang, Bai and Yang was supported by the NSF/CTS under grant 9873236, and by the Engineering Research Programs at the Office of Basic Energy Science of the DOE.

References

- Balmer, R.T. The hydrocyst—a stability phenomenon in continuum mechanics, *Nature* (London) **227**, 600 (1970).
- Bowden, N., I.S. Choi, B.A. Grzybowski, G.M. Whitesides, Mesoscale self-assembly of hexagonal plates using lateral capillary forces: synthesis using the “capillary bond”, *J. Am. Chem. Soc.* **121**, 5373-5391. (1999).
- Bowden, N., A. Terfort, J. Carbeck, G.M. Whitesides, Self-assembly of mesoscale objects into ordered two-dimensional arrays, *Science*, **276**, 233-235. (1997).
- Brenner, H. and L.G. Leal. A micromechanical derivation of Fick’s law for interfacial diffusion of surfactant molecules, *J. Colloid Interface Sci.* **65**, 191 (1978).
- Brenner, H. and L.G. Leal. Conservation and constitutive equations for adsorbed species undergoing surface diffusion and convection at a fluid-fluid interface, *J. Colloid Interface Sci.* **88**, 136 (1982).
- Chan, D.Y.C., J.D. Henry Jr. and L.R. White. The interaction of colloidal particles collected at the fluid interface, *J. Colloid Interface Sci.* **79**, 410 (1981).
- Danov, K.D., R. Aust, F. Durst and U. Lange. Influence of the surface viscosity on the hydrodynamic resistance and surface diffusivity of a large Brownian particle, *J. Colloid and Interface Science*, **175**(1), Oct 36-45 (1995).
- Fortes, M.A. Attraction and repulsion of floating particles, *Can. J. Chem.* **60**, 2889 (1982).
- Gifford, W.A. and L.E. Scriven. On the attraction of floating particles, *Chem. Engrg. Sci.* **26**, 287-297 (1971).
- Goldman, A.J., R.G. Cox and H. Brenner. Slow viscous motion of a sphere parallel to a plane wall—I Motion through a quiescent fluid, *Chem. Eng. Sci.* **22**, 637-651 (1967).
- Govindarajan, R., P.R. Nott, and S. Ramaswamy. Theory of suspension segregation in partially filled horizontal rotating cylinders, *Phy. Fluids*, **13**(12), 3517-3520 (2001).

- Grzybowski, B.A., N. Bowden, F. Arias, H. Yang, G.M. Whitesides, Modeling of menisci and capillary forces from the millimeter to the micrometer size range, *J. Phys. Chem. B* **105**, 404-412. (2001).
- Joseph, D.D., M. Arney, G. Ma, 1992. Upper and lower bounds for interfacial tension using spinning drop devices, *J. Colloid Interface Sci.*, **148**(1), 291-294.
- Karweit, M.J. and S. Corsin. Observation of cellular patterns in a partly filled, horizontal, rotating cylinder, *Phys. Fluids* **18**, 111 (1975).
- Kato, K., H. Fujita and E. Imazu. Motion of a particle floating on a liquid meniscus surface, *J. Fluids Engrg.* **114**, 411 (1992).
- Kralchevsky, P.A., V.N. Paunov, N.D. Denkov, I.B. Ivanov and K. Nagayama. Energetical and force approaches to the capillary interactions between particles attached to a liquid-fluid interface, *J. Colloid and Interface Sci.* **155**, 420-437 (1993).
- Kralchevsky, P.A., V.N. Paunov, I.B. Ivanov and K. Nagayama. Capillary meniscus interactions between colloidal particles attached to a liquid-fluid interface, *J. Colloid Interface Sci.* **151**, 79 – 94 (1992).
- Kralchevsky, P.A. and K. Nagayama. Capillary interactions between particles bound to interfaces, liquid films and biomembranes, *Advances in Colloid and Interface Sci.* **85**, 145-192 (2000).
- Majumdar, S.R., M.E. O'Neill, and H. Brenner. Note on the slow rotation of a concave spherical lens or bowl in two immiscible semi-infinite viscous fluids, *Mathematika*, **21**, 147-154 (1974).
- Nicolson, M.M. The interaction between floating particles, *Proc. Cambridge Philosophical Soc.*, **45**, 288 (1949).
- Petkov, J.T., N.D. Denkov, K.D. Danov, O.D. Velev, R. Aust and F. Durst. Measurement of the drag coefficient of spherical particles attached to fluid interfaces, *J. Colloid and Interface Science*, **172**, 147-154 (1995).
- Poynting, J.H. and J.J. Thompson. *A Text-book of Physics: Vol. 1, Properties of Matter*, C. Griffith & Co. Ltd (London) 153-155 (1913).
- Preziosi, L. and D.D. Joseph. The run-off condition for coating and rimming flows, *J. Fluid Mech.*, **187**, 99-113 (1988).
- Princen, H.M. Equilibrium shape of interfaces, drops, and bubbles. Rigid and deformable particles at interfaces, *Surface and Colloid Science*, E. Matijevic, ed., Interscience, New York, Vol. 2, p.1-84 (1969).
- Rapacchietta, A.V. and A.W. Neumann. Force and free-energy analyses of small particles at fluid interfaces: II. Spheres, *J. Colloid and Interface Sci.*, **59**(3), 555-567 (1977).
- Redoev, B., M. Nedjalkov and V. Djakovich. Brownian motion at liquid-gas interfaces. 1. Diffusion coefficients of macroparticles at pure interfaces, *Langmuir*, **8**, 2962 (1992).
- Ruschak, K.J. and L.E. Scriven, Rimming flow of liquid in a rotating horizontal cylinder, *J. Fluid Mech.* **76**, 113-127 (1976).

- Saif, T.A., On the capillary interaction between solid plates forming menisci on the surface of a liquid, *J. Fluid Mech.* in press (2002).
- Schneider, Y.C., M.E. O'Neill, and H. Brenner. On the slow viscous rotation of a body straddling the interface between two immiscible semi-infinite fluids, *Mathematika*, **20**, 175 (1973).
- Timberlake, B.D., J.F. Morris, Concentration band dynamics in free-surface Couette flow of a suspension, *Phy. Fluids*, 14(5), 1580-1589 (2002).
- Tirumkudulu, M., A. Tripathi, A. Acrivos. Particle segregation in monodisperse sheared suspensions, *Phy. Fluids*, **11**(3), 507-509 (1999).
- Tirumkudulu, M., A. Mileo, A. Acrivos. Particle segregation in monodisperse sheared suspensions in a partially filled rotating horizontal cylinder, *Phy. Fluids*, **12**(6), 1615 (2000).
- Tirumkudulu, A. Acrivos. Coating flows within a rotating horizontal cylinder: Lubrication analysis, numerical computations, and experimental measurements, *Phys. Fluids*, **13**, 3517 (2001).
- Vonnegut, B., Rotating Bubble Method for the Determination of Surface and Interfacial Tension, *Rev. Sci. Instrum.* **13**, 6-9, (1942).
- Wakiya, S. *Niigata Univ. College of Engng. Res. Rept.* 6, Nagoaka, Japan (30 March 1957).

Table of contents

Abstract	1
I. Capillary forces	1
I-1. Vertical forces	2
I-2. Horizontal forces	4
I-3. Particle clustering	7
II. Particle aggregation in a liquid film rimming a rotating cylinder	11
II-1. The ratio of the minimum film thickness to the particle diameter	12
II-2. Particle segregation in aqueous Triton mixtures	15
II-3. Particle segregation in water	20
II-4. Particle segregation in glycerin	21
III. Particle segregation due to the formation of bubbles:	22
III-1. Bubbles in a partially filled rotating cylinder:	23
III-2. Particles segregation due to bubbles:	26
III-3. Segregation of bi-disperse suspension in a partially filled rotating cylinder	29
IV. Conclusion	30
References	32